RSC Advances

PAPER

Cite this: *RSC Adv.*, 2020, **10**, 26443

New possible candidate structure for phase IV of solid hydrogen†

Guo-Jun Li,[ab] Yun-Jun Gu,[b] Zhi-Guo Li,[b] Qi-Feng Chen*[b] and Xiang-Rong Chen*[a]

It has been proved in experiments that there are at least five phases of solid hydrogen at high pressure, however, only the structure of phase I has been absolutely determined. We revisited the phase space of solid hydrogen in the pressure range of 200–500 GPa using the particle swarm optimization technique combined with first-principles simulations. A novel orthorhombic structure named *Ama*2 is proposed as a possible candidate structure for phase IV. The *Ama*2 structure is a 'mixed structure' with two different types of layers and is distinctly different from the previously reported *Pc* structure. Enthalpies and Gibbs free energies show that *Ama*2 and *Pc* are competitive in the pressure region of phase IV. Nevertheless, the Raman and infrared vibron frequencies of *Ama*2 calculated by using density functional perturbation theory based on first-principles lattice dynamics show a better agreement with the experimental measurements than those of the *Pc* structure. And the pressure dependence of these low-frequency Raman vibrons of *Ama*2 obtained from the first-principles molecular dynamics simulation shows a steeper slope, which resolves the long-standing issue of large discrepancies between the calculated Raman frequencies and the experimental ν_1 [P. Loubeyre, F. Occelli and P. Dumas, *Phys. Rev. B: Condens. Matter Mater. Phys.*, 2013, **87**, 134101 and C. S. Zha, R. E. Cohen, H. K. Mao and R. J. Hemley, *Proc. Natl. Acad. Sci. U.S.A.*, 2014, **111**, 4792]. Structural and vibrational analyses show that the hydrogen molecules in the weakly bonded molecular layer of *Ama*2 form distorted hexagonal patterns, and their vibration can be used to explain the experimental ν_1 vibron. It is found that the weakly bonded layer is almost the same as the layers in the *C*2/*c* structure. This confirms the experimental conclusion [P. Loubeyre, F. Occelli and P. Dumas, *Phys. Rev. B: Condens. Matter Mater. Phys.*, 2013, **87**, 134101] that the ordering of hydrogen molecules in the weakly bonded molecular layers of the 'mixed structure' for phase IV is similar to that in the layers of the *C*2/*c* structure.

Received 10th August 2019
Accepted 29th June 2020

DOI: 10.1039/d0ra03295f

rsc.li/rsc-advances

1 Introduction

Although the hydrogen atom consists of a single proton and electron, it exhibits complex behavior under high pressure, especially in the solid phase. Since Wigner and Huntington predicted that solid hydrogen transforms into a metallic atomic crystal above 25 GPa,[1] it has attracted wide attention in theory and experiments due to the importance of developing and testing computer simulation methods, as well as its relevance to astrophysics.[2] Later, some important quantum effects were also predicted, such as a metallic liquid ground state at high pressure and low temperature,[3,4] high-T_c superconductivity,[5–7] and metallic superfluid and superconducting superfluid states.[8,9]

Early static diamond anvil cell (DAC) experiments showed that there were three different low temperature phases of solid hydrogen.[2,10,11] Phase I is a molecular solid of quantum rotors, which adopts a hexagonal close packed lattice. It transforms into the broken-symmetry phase II at about 110 GPa. Phase III is characteristic of a large discontinuity in the vibron frequency, and exists above 150 GPa. Due to the development of static compression technologies, more phases of solid hydrogen have been recently discovered at higher temperatures and pressures. Phase IV, discovered at 300 K and above 220 GPa, exhibits a distinctly different spectrum compared with phase III, and has two vibron frequencies in its Raman and infrared (IR) spectra. The structure of phase IV is inferred as an anisotropic, mixed layer structure.[12–14] Similarly, a series of new possible phases of solid hydrogen were proposed according to the change in the optical spectrum.[15–17]

Because of the very weak X-ray scattering by hydrogen atoms and small sample sizes, until now the only structure of solid hydrogen determined clearly by experimental measurements is the hexagonal close packed lattice of phase I.[2] Therefore, much effort has been directed toward searching for candidate

[a]*College of Physics, Sichuan University, Chengdu 610065, China. E-mail: xrchen@scu.edu.cn*

[b]*National Key Laboratory for Shock Wave and Detonation Physics Research, Institute of Fluid Physics, China Academy of Engineering Physics, Mianyang 621900, China. E-mail: chenqf01@gmail.com*

† Electronic supplementary information (ESI) available: The structural information for the *Ama*2 phase, vibrational analysis, the FPMD details, and the pressure dependence of the bond lengths are given. See DOI: 10.1039/d0ra03295f

structures of solid hydrogen by combining DFT with optimization algorithms at high pressures and low temperatures, which has improved our understanding of the experimental observations[18–22] and predicted some peculiar properties for hydrogen at pressures beyond those explored experimentally.[23–26] The *C*2/*c* structure was proposed for phase III above 200 GPa and its Raman and IR vibrons exhibit good agreement with the experimental observations. Compared with phase III, the experimental Raman (infrared) spectrum of phase IV is more complex, and has two distinct vibron frequencies. This indicates a more complex structure for phase IV. The 'mixed structure' *Pbcn* was first proposed to explain the experimental Raman spectrum of phase IV.[13] Later, Pickard *et al.* suggested that the 'mixed structure' *Pc* was more suitable for phase IV, because *Pc* was more stable than *Pbcn* based on the phonon dispersion calculations.[20] The 'mixed structure' of *Pc*, characterized by two distinctly different layered structures, can qualitatively explain the two Raman and IR vibron peaks observed in phase IV. Nevertheless, the calculated values of the vibron frequencies are far from the experimentally measured values for phase IV. This may arise from significant differences between the *Pc* structure and the real structure.[27,28] Moreover, Azadi *et al.*[29] found that finite temperature and nuclear quantum effects, in addition to a strongly correlated band-gap energy and vibron modes, can reduce the band-gap substantially so that the *Pc* structure enters a metallic state, which is inconsistent with most experimental evidence. They concluded that the *Pc* structure was not a good candidate for phase IV. However, the recent single-crystal X-ray diffraction experiments of solid hydrogen indicate that the transitions from phase I to phases III and IV are possible an isostructural phase transition.[30] Hence, for the structural model of phase IV, theoretical studies and experimental measurements have not yet achieved consistent conclusions.

It should also be mentioned that previous structure predictions were generally based on the potential energy surface calculated using the Perdew–Burke–Ernzerhof (PBE) functional.[31] Recent theoretical calculations showed that the phase transition and metallization pressure of solid hydrogen strongly depended on the exchange–correlation (XC) functional.[32–34] The XC functionals that take into account the van der Waals (vdW) interactions, such as optB88-vdW,[35] vdW-DF1,[36] and vdW-DF2,[37] have an important effect on the phase stability and transition pressure of solid hydrogen, reducing further the discrepancy between the theoretical and experimental phase diagrams compared with the PBE functional.[33,34,38,39]

Given the above considerations, it is necessary to revisit the candidate structures for phase IV. The particle swarm optimization (PSO) technique has been demonstrated as a successful method to predict stable or metastable structures of various systems under the given external conditions (pressure).[24,25,40–42] PSO combined with first-principles total energy calculations adopting the vdW-DF2 functional are used to search extensively and systematically for possible candidate structures at pressures from 200 GPa to 500 GPa. An orthorhombic structure named *Ama*2 is proposed as a possible candidate for phase IV, whose energy is competitive with that of the *Pc* structure. Furthermore, the properties of phonon dispersion, bond length, vibration mode, Raman spectra , and infrared spectra for *Ama*2 were studied in detail. The paper is organized as follows. The calculation method and details are described in Section 2. Section 3 presents the results and discussion. The final conclusions are presented in Section 4.

2 Method

We combined the PSO technique within the evolutionary scheme as implemented in CALYPSO code[40,43] with first-principles total energy calculations achieved with the Vienna *Ab initio* Simulation Package (VASP)[44] to search for structures of solid hydrogen. All 1200 simulation cells with 48 atoms per cell were produced at 300 GPa by the CALYPSO code during the structure evolution, which is enough to ensure convergence of the searched structures. This search was repeated at pressures of 400 GPa and 500 GPa. In the structure relaxations and electronic calculations, the projector augmented-wave (PAW) potential[45,46] was adopted and the exchange–correlation functional was described by the vdW-DF2 functional. The basis set of plane waves with energy cutoff 1200 eV and the Monkhorst–Pack[47] Brillouin zone sampling with a *k*-point grid with spacing 0.2 Å^{-1} were found to be sufficient for electronic structure calculation and structure relaxation. The convergence of total energy and force were set to less than 0.001 meV per proton and 0.1 meV Å^{-1}, respectively.

Force constants calculated with density functional perturbation theory (DFPT)[48,49] were processed using the Phonopy code[50] to get the phonon dispersion relation. In the dynamical matrix calculation, the value of the energy cutoff and the size of the *k*-point grid were the same as in the electronic structure calculation. Then, the vibrational free energy was calculated on a denser Monkhorst–Pack grid with a size of 41 × 41 × 41, which ensured that the vibration free energy converged to 0.01 meV per proton. To ensure that the zero-point (ZP) vibration energy (E_{ZP}) variation of all calculated structures converged to 0.1 meV per proton, a supercell with 96 atoms was adopted for the *Ama*2, *C*2/*c*, *Pbcn*, and *Pc* structures, while supercells with 144 and 128 atoms were adopted for the *Cmca*-12 and *Cmca*-4 structures, respectively (see Table S1 of the ESI† for more details). The total E_{ZP} and Gibbs free energy *G* of the candidate structures were calculated according to the harmonic approximation,

$$E_{ZP} = \frac{1}{2}\sum_{q,j}\hbar\omega_{q,j} \quad (1)$$

$$G = U + PV + E_{ZP} + k_B T\sum_{q,j}\ln\left[1 - \exp\left(\hbar\omega_{q,j}\right)/k_B T\right] \quad (2)$$

where $\omega_{q,j}$ is the phonon frequency of the *j*th mode at wave vector *q* in the Brillouin zone, $\hbar$ is the Planck constant divided by 2π, *U* is the electronic energy of a static nucleus, k_B is the Boltzmann constant, and *V* and *P* are the volume of the structure and the external pressure, respectively.

The Raman and IR spectra of solid hydrogen were calculated with the CASTEP code using the DFPT method based on first-principles lattice dynamics (LD) calculations.[51] The PBE

functional and norm-conserving pseudo-potentials, which were generated from the optimization scheme of Lin *et al.*,[52] were adopted. The Raman spectra of the *Ama*2 structure were calculated using the vdW-DF2 functional within VASP code and post-processed with a python script.[53,54]

3 Results and discussion

3.1 *Ama*2 structure and relative stability

We found a series of low-energy structures (except for the *Pbcn* structure) that had been proposed in previous work.[18–20] In addition, a new candidate *Ama*2 structure (space group 40) named as its short Hermann–Mauguin space-group symbol is found for the first time and has 24 atoms in the primitive unit cell. Due to the constraints of the periodic boundary conditions, layer A seems to split into two layers, but in fact, it all belongs to the same layer which is similar to layer C, as shown in Fig. 1. Therefore, *Ama*2 adopts an ABCDA… structure (see Table S2 of the ESI† for more detailed structural information). *Ama*2 has two distinct types of layers and is a 'mixed structure'. One type of layer consists of weakly bonded hydrogen molecules (labeled as layers B and D) forming distorted hexagonal patterns (Fig. 1(c)) that can also be found in the *C*2/*c* structure, but are different from the graphene-like weakly bonded molecular layers in *Pc*.[55] The other type of layer contains strongly bonded molecules (labeled as layers A and C) forming highly distorted hexagonal patterns (Fig. 1(d)). Therefore, *Ama*2 is completely different from *Pc* and *Pbcn*, and provides another possible arrangement of hydrogen molecules (H_2) in solid hydrogen.

At the static lattice level, the relative enthalpies of the candidate structures calculated by the vdW-DF2 functional are illustrated in Fig. 2(a). *C*2/*c* is the most stable structure and *Cmca*-4, considered as the metallic molecular phase, always has the highest enthalpy within the pressure range of 200–500 GPa. It is noted that the difference in enthalpy between *Pc* and *Ama*2 is smaller than 1 meV per proton above 250 GPa. Besides, the *Ama*2 phase is more competitive than *Pbcn* in the range 200–500 GPa. Phase IV of solid hydrogen occurs above 220 GPa, and *Pc* and *Pbcn* were both considered as candidate structures in previous literature.[13,20] Based on the above comparison of the calculated energies, *Ama*2 can also be a candidate structure for phase IV. In order to investigate the effects of different XC functionals, we calculated the energies of the candidate structures at the static lattice level using the PBE functional, as shown in Fig. 2(b). The general trends in the energies for different structures coincide with the results of Pickard *et al.*,[18]

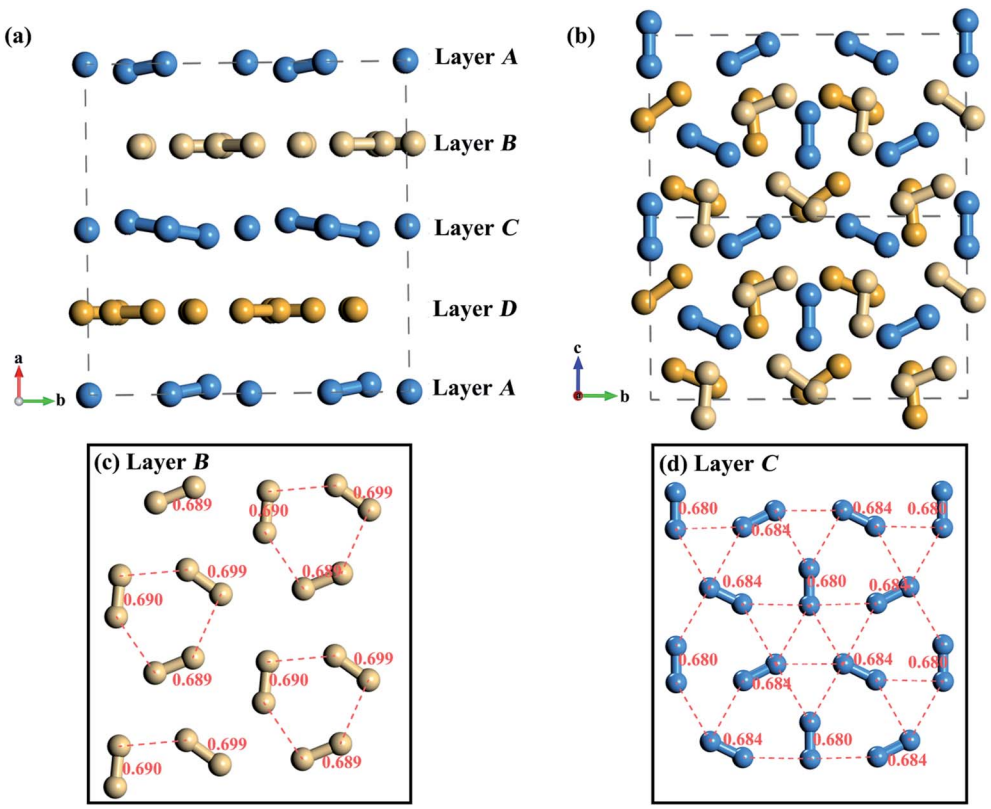

Fig. 1 The *Ama*2 structure (supercell with 96 atoms along the *c* axis) calculated by using the vdW-DF2 functional at 300 GPa. Numbers and red dashed lines in (c) and (d) represent the bond lengths and close contacts between atoms which are smaller than 1.2 (1.31) Å, respectively. Based on the bond lengths of the hydrogen molecules contained in the layers, layers A and C are classified as strongly bonded molecular layers, and layers B and D are classified as weakly bonded molecular layers. (a) The view of the *Ama*2 structure along the *c* axis. (b) The view of the *Ama*2 structure along the *a* axis. (c) The weakly bonded molecular layers where the molecules lie flat within a plane and form a distorted hexagonal pattern, similar to the layers in *C*2/*c*. (d) In the strongly bonded molecular layers, there are two different bond lengths which are 0.680 and 0.684 Å. Hydrogen molecules form a highly distorted hexagonal pattern, which seems to be similar to the layers in *Cmca*-12.

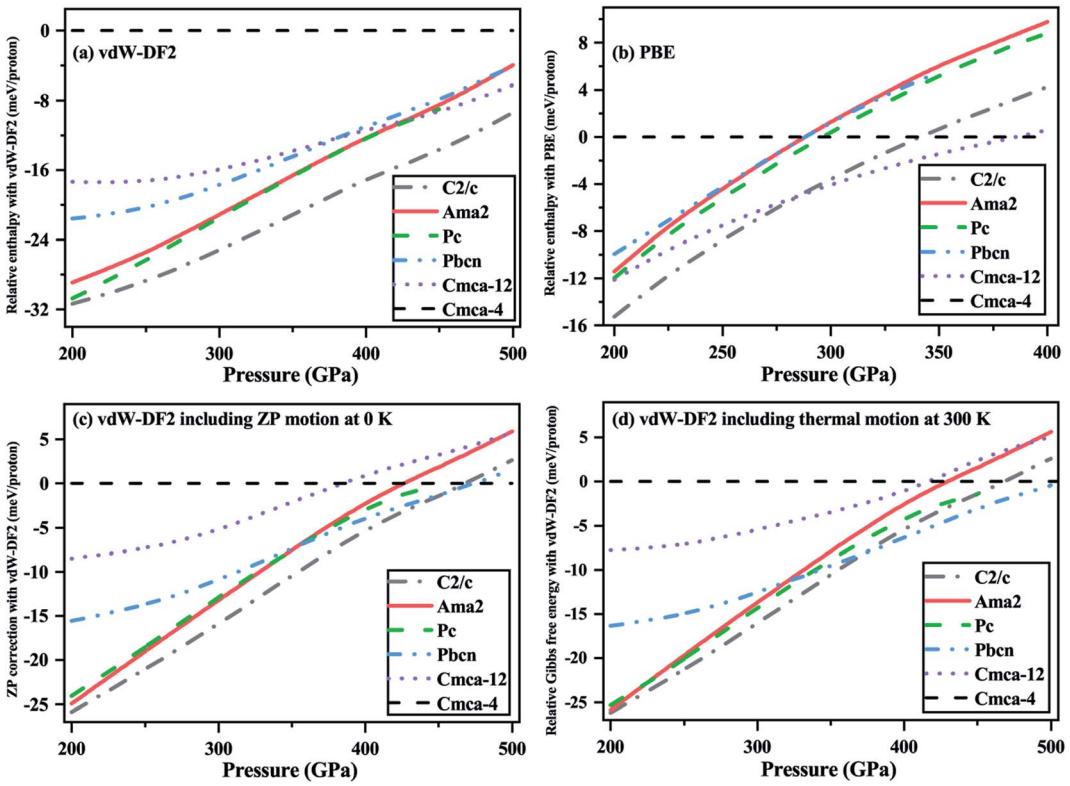

Fig. 2 Enthalpies without and with ZP correction, and the Gibbs free energies of the *Cmca*-12 (purple short dashed line), *Pbcn* (blue dash-dot line), *Pc* (green dashed line), *Ama*2 (red solid line), and *C*2/*c* (gray dash-dot line) structures with respect to those of *Cmca*-4 (black dashed line). (a) and (b) present energies of the static lattice structures calculated using the vdW-DF2 and PBE functionals, respectively. Energies of the static lattice with proton ZP motion correction and Gibbs free energies calculated with the vdW-DF2 functional at 300 K are presented in (c) and (d), respectively.

but are different from the results obtained with vdW-DF2 calculations. Compared with *Pc*, *Ama*2, and *Pbcn*, *Cmca*-12 is energetically uncompetitive at the vdW-DF2 level, but gets more competitive at the PBE level. The PBE calculations also show that *Pc* exhibits a slight energetic advantage compared with *Ama*2 and *Pbcn*, however, the energy difference between *Ama*2, *Pc*, and *Pbcn* is really small. All in all, the different XC functionals have an effect on the relative stability order of the candidate structures. Nevertheless, the PBE and vdW-DF2 calculations both show that the static lattice energies of *Ama*2 and *Pc* differ very little.

Due to the small mass of hydrogen nuclei, a strong ZP motion is expected. When the ZP vibrational energy is added to the static lattice energy, as illustrated in Fig. 2(c), *C*2/*c* remains stable below 453 GPa, which agrees with the previous predictions by diffusion Monte Carlo (DMC) calculations[34] and the recent infrared spectroscopic measurements.[56] The *Ama*2 structure is more competitive energetically compared with *Pc* and *Pbcn* below 345 GPa, whereas the *Pbcn* phase has the lowest energy compared with *Ama*2 and *Pc* above 355 GPa. As phase IV was discovered at 225 GPa and 300 K experimentally, we calculated the Gibbs free energies for these structures at 300 K within the harmonic approximation and focused on the difference in energy between the *Ama*2, *Pbcn*, and *Pc* structures. As shown in Fig. 2(d), owing to lattice vibration contributing to the global energy of the candidate structures, the pressure at which *C*2/*c* transforms to the *Pbcn* phase is reduced to 370 GPa. The difference in Gibbs free energy between *Pc* and *Ama*2 is smaller than about 1 meV, and *Pbcn* is energetically uncompetitive compared with *Pc* and *Ama*2 in the range of 200–320 GPa. The differences between *Pc*, *Pbcn*, and *Ama*2 become obvious above 350 GPa. In general, under the four different conditions considered above, *Ama*2 has relatively low energies, and is energetically degenerate with the previously highlighted *Pc* structure, especially for the pressure region of 200–350 GPa. Therefore, *Ama*2 is a possible candidate structure for phase IV from an energy point of view.

3.2 Phonon spectra

Phonon dispersion relations can be used to identify the stability of a candidate structure of solid hydrogen. Here, we depict the phonon dispersion relations of the *C*2/*c*, *Ama*2, *Pc*, and *Pbcn* phases at 300 GPa according to the harmonic approximation in Fig. 3. The *Ama*2 phase has no imaginary frequencies along the high symmetry point in the Brillouin zone, which suggests that the *Ama*2 structure is dynamically stable. But the *Pc* and *Pbcn* structures have negative frequencies in the vicinity of some high symmetry points, and the *Pbcn* phase has more unstable modes in reciprocal space than the *Pc* phase as suggested by Pickard *et al.*[20] Based on a large number of phonon dispersion

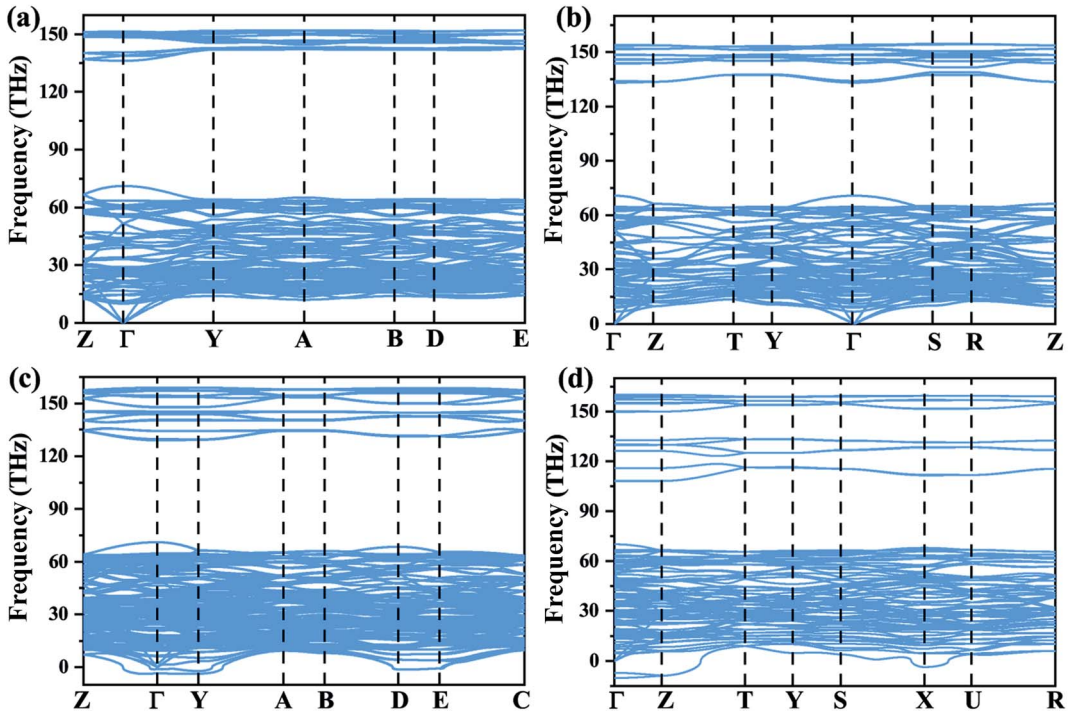

Fig. 3 Phonon dispersions of (a) *C*2/*c*, (b) *Ama*2, (c) *Pc*, and (d) *Pbcn* calculated by using the vdW-DF2 functional at 300 GPa.

calculations, the *Ama*2 phase is stable over the investigated pressure range of 250–500 GPa, whereas *Pc* is unstable. Therefore, in terms of the phonon dispersion properties, *Ama*2 seems to be more competitive than the *Pc* structure for phase IV. To further confirm these structures, the Raman and IR properties of the *Pc* and *Ama*2 structures should be examined against the experimentally measured data, which will be discussed in detail in the next section.

3.3 Raman and IR spectra

Raman and infrared spectroscopy are crucial tools for identifying the candidate structures of phase IV. In Fig. 4 we show the Raman spectra of *Ama*2 at 300 GPa calculated by LD and the molecular projection method based on first-principles molecular dynamics (FPMD) simulations,[57–59] together with the experimental Raman spectrum at 303 GPa. The FPMD calculation details can be found in the ESI.† At the LD level, the Raman spectra of *Ama*2 at 300 GPa calculated by vdW-DF2 and PBE are used to illustrate the dependence of the peak positions on the XC functional. Both functionals predict that *Ama*2 has two strong Raman vibron modes, which are consistent with the two intense Raman vibrons observed in experiments for phase IV.[12,13,28] Based on the vibrational analysis, the lower and higher frequencies of Raman vibrons correspond to the hydrogen molecular vibrations of weakly bonded molecular layers and strongly bonded molecular layers, respectively (see Fig. S1 in the ESI†). The Raman vibron frequencies estimated by PBE are obviously smaller than those predicted by vdW-DF2. The lower and higher Raman vibron frequencies calculated by PBE and vdW-DF2 at 300 GPa are 3182/3939 and 4461/4817 cm^{-1}, respectively. This is closely related to the bond lengths (BLs) calculated by PBE and vdW-DF2. The BLs of *Ama*2 calculated by the PBE functional are larger than those calculated by the vdW-DF2 functional. For instance, at 300 GPa, the BLs in the weakly (strongly) bonded molecular layers of *Ama*2 are 0.689/0.699 (0.68/0.684) Å according to vdW-DF2 and 0.766/0.78 (0.73/0.735) Å according to PBE (see the ESI† for more details). These results confirm the empirical formula relating the Raman frequency and bond length r, *i.e.* $\nu r^3 =$ constant.[13] Although the results calculated by the PBE functional seem to be more reasonable than those calculated by the vdW-DF2 functional, the results still disagree with the experimental observation to some extent. This is due to the fact that the LD method, which is used to calculate the Raman spectrum at 0 K, doesn't include the anharmonic effect (finite-temperature effect) on the proton. The FPMD method can effectively include the finite-temperature effect. Therefore, the Raman peaks calculated by the FPMD method coincide with the experimental measurement very well. And the experimentally broadened linewidth of the ν_1 vibron[12,13,28] is also captured by the FPMD method (see Fig. S2 in the ESI† for more details).

Moreover, we used the LD method to calculate the pressure dependence of the Raman and IR vibron frequencies of *Ama*2 and the other candidate structures, which are compared with experimental measurements. The Raman and IR spectra of the *Ama*2 structure calculated at different pressures are depicted in Fig. S4,† and the derived pressure dependence of the vibron frequencies is presented in Fig. 5 (see Fig. S5† for the pressure dependence of low-frequency Raman frequencies). It is noted that the calculated IR intensity ratio between the two vibrons of *Ama*2 (see Fig. S4†) is inverse to the experimental one.[27] This

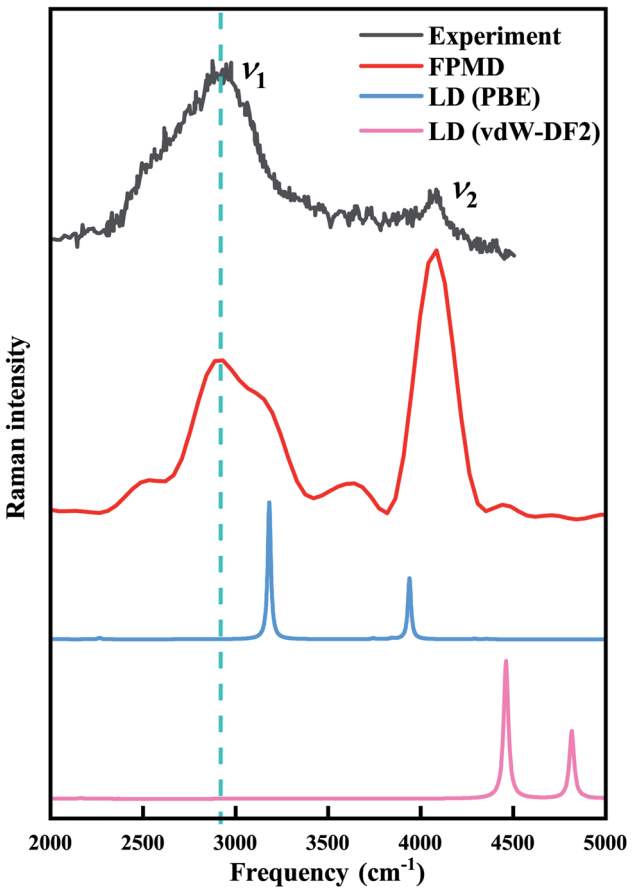

Fig. 4 Raman peaks of *Ama*2 compared with the experimental measurements. Raman peaks were calculated at 0 K and 300 GPa by the LD method using vdW-DF2 (pink line) and PBE (blue line). Raman peaks (red line) were calculated at 220 K and 300 GPa using the molecular projection method FPMD. Experimental data at 303 GPa and room temperature (black line) are taken from Zha *et al.*[28] When the detected Raman frequency is higher, the sensitivity of the experimental detection device is lower, so the calculated vibronic amplitudes are not compared directly to the experimental measurements.[13,57] The dashed line guides the eyes.

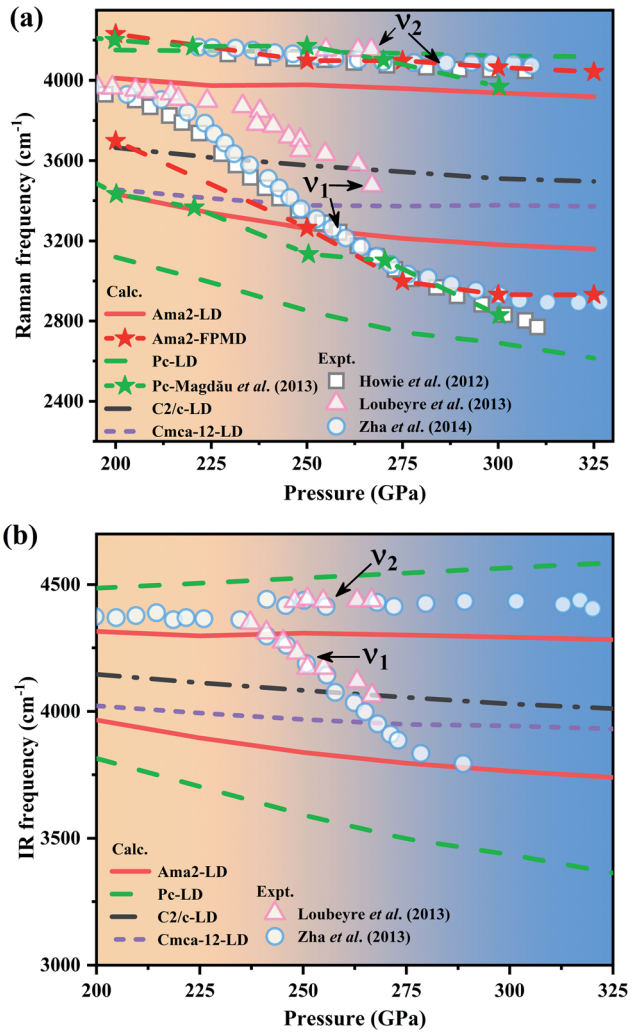

Fig. 5 Pressure dependence of (a) Raman and (b) IR vibron frequencies of solid hydrogen. LD calculations were performed at 0 K for *Ama*2 (red solid line), *Pc* (green dashed line), *C*2/*c* (gray dash-dot line), and *Cmca*-12 (purple short dashed line). FPMD calculations were performed for *Ama*2 (red stars) at 220 K. Raman vibron frequencies of *Pc* (green stars) are taken from data calculated at 220 K by Magdău and Ackland.[57] Experimental data are taken from Howie *et al.*[13] (gray open squares), Loubeyre *et al.*[27] (pink open triangles), and Zha *et al.*[28] (blue open circles).

may be because the IR spectra calculated by LD don't include the temperature effect. Below about 220 GPa, both Raman and IR measurements show only one vibronic frequency labeled as ν_1 for phase III. The experimental vibronic frequency ν_2 occurs above 225 GPa in the Raman and IR spectra and is identified as a signal of the transition from phase III to phase IV. Both the *Pc* and *Ama*2 structures have two intense vibrons in the Raman and IR spectra, whereas *Cmca*-12 and *C*2/*c* have only one intense vibron and can be excluded from the candidate structures of phase IV. For the lower-frequency vibron ν_1, the calculated Raman and IR frequencies of *Pc* are lower than the experimental frequencies, especially for IR. This is probably because the coupling between the hydrogen molecules in the graphene-like weakly bonded layers of the *Pc* structure was overestimated, as suggested by Loubeyre *et al.*[27] The low-frequency Raman and IR ν_1 vibrons of *Ama*2 are close to those of *C*2/*c* and *Cmca*-12 (all of them consist of layers with H_2 molecules forming distorted hexagonal patterns), and are better reproductions of the experimental observations than those of *Pc*. But the slope of the Raman ν_1 vibron of *Ama*2 is still too flat. This is because LD calculations do not include the finite-temperature effect. The FPMD calculations are more consistent with the experimental measurements and provide a steeper slope for the Raman ν_1 vibron of *Ama*2. The high-frequency Raman ν_2 vibron of *Ama*2 calculated with FPMD perfectly reproduces the experimental observations, whereas the results of the LD calculations are smaller than the experimental results. The huge difference between the two methods confirms the experimental conclusion[13] that the finite-temperature effect is a crucial factor for phase IV. Moreover, the frequencies of the *Ama*2 ν_1 vibron calculated by FPMD show a better agreement with the experimental data compared with those of the *Pc* structure. This arises

from the slight difference in molecule arrangement between *Ama*2 and *Pc* at a finite-temperature. To some extent, the Raman and IR properties of *Ama*2 narrow the gap between theoretical calculations and experiments.

4 Conclusion

In this work, we revisited the phase space of solid hydrogen in the pressure range of 200–500 GPa by combining the particle swarm optimization technique and first-principles energy calculations. The *Ama*2 structure was proposed as a possible candidate structure for phase IV of solid hydrogen. The new structure shares features of the *C*2/*c*, *Cmca*-12, *Pc*, and *Pbcn* structures. *Ama*2 adopts a 'mixed structure' and has two types of layers. This feature is consistent with the previously highlighted *Pc* and *Pbcn* structures. One type of layer with weakly bonded molecules forms distorted hexagonal patterns, which is almost the same as the layers in the *C*2/*c* structure. The other type of layer contains strongly bonded molecules which form highly distorted hexagonal patterns and non-hexagonal patterns. Moreover, the frequencies of the Raman and IR ν_1 vibron of *Ama*2, arising from the vibrations of the weakly bonded molecular layers, agree better with the experimental ν_1 frequencies than those of *Pc*. The features of the *Ama*2 structure confirm the experimental conclusion of Loubeyre *et al.*[27] that the ordering of hydrogen molecules in the weakly bonded molecular layers of 'mixed structures' of phase IV is similar to that in the layers in the *C*2/*c* structure. The pressure dependent Raman ν_1 vibron of *Ama*2 obtained from FPMD has a steeper slope and is more consistent with the experimental ν_1. Phase IV is believed to exhibit strong quantum effects for the protons and a single classical structure may not fully describe phase IV.[28] The *Ama*2 structure is a good addition to the structure model for phase IV in view of the DFT calculations. Moreover, it should be noted that the *C*2/*c* structure is more energetically stable than *Pc* and *Ama*2 within the pressure and temperature ranges of phase IV according to the DFT simulation. However, more advanced DMC calculations including anharmonic corrections stabilize the *Pc* structure.[55] Therefore, further work will focus on investigating the stability of *Ama*2 and *Pc* by using the more advanced method.

Conflicts of interest

There are no conflicts to declare.

Acknowledgements

We thank Hua Y. Geng for valuable discussion. This work is supported by the Foundation of National Key Laboratory of Shock Wave and Detonation Physics (Grant No. 6142A0301020217, and JCKYS2018212001), the National Natural Science Foundation of China (Grant No. 11872057, 11802280, and 11674292), the Science Challenge Project (Grant No. TZ2016001), the Science and Technology Development Foundation of China Academy of Engineering Physics (Grant No. 2013A0101001, and 2015B0102001), the NSAF (Grant No. U1830101), the Youth Program of National Natural Science Foundation of China (11804284) and the Foundation and Frontier Research Project of Chongqing (cstc2017jcyjAX0308). We are particularly grateful for the computational resources of the TianHe-2 at the LvLiang Cloud Computing Center of China.

References

1 E. Wigner and H. B. Huntington, *J. Chem. Phys.*, 1935, **3**, 764–770.
2 J. M. McMahon, M. A. Morales, C. Pierleoni and D. M. Ceperley, *Rev. Mod. Phys.*, 2012, **84**, 1607–1653.
3 S. A. Bonev, B. Militzer and G. Galli, *Phys. Rev. B: Condens. Matter Mater. Phys.*, 2004, **69**, 014101.
4 S. Deemyad and I. F. Silvera, *Phys. Rev. Lett.*, 2008, **100**, 155701.
5 N. W. Ashcroft, *Phys. Rev. Lett.*, 1968, **21**, 1748–1749.
6 P. Cudazzo, G. Profeta, A. Sanna, A. Floris, A. Continenza, S. Massidda and E. K. Gross, *Phys. Rev. Lett.*, 2008, **100**, 257001.
7 J. M. McMahon and D. M. Ceperley, *Phys. Rev. B: Condens. Matter Mater. Phys.*, 2011, **84**, 144515.
8 S. A. Bonev, E. Schwegler, T. Ogitsu and G. Galli, *Nature*, 2004, **431**, 669–672.
9 E. Babaev, A. Sudbø and N. W. Ashcroft, *Phys. Rev. Lett.*, 2005, **95**, 105301.
10 I. F. Silvera, *Rev. Mod. Phys.*, 1980, **52**, 393–452.
11 H.-k. Mao and R. J. Hemley, *Rev. Mod. Phys.*, 1994, **66**, 671–692.
12 M. I. Eremets and I. A. Troyan, *Nat. Mater.*, 2011, **10**, 927–931.
13 R. T. Howie, C. L. Guillaume, T. Scheler, A. F. Goncharov and E. Gregoryanz, *Phys. Rev. Lett.*, 2012, **108**, 125501.
14 C. S. Zha, Z. Liu and R. J. Hemley, *Phys. Rev. Lett.*, 2012, **108**, 146402.
15 R. T. Howie, T. Scheler, C. L. Guillaume and E. Gregoryanz, *Phys. Rev. B: Condens. Matter Mater. Phys.*, 2012, **86**, 214104.
16 P. Dalladay-Simpson, R. T. Howie and E. Gregoryanz, *Nature*, 2016, **529**, 63–67.
17 R. T. Howie, P. Dalladay-Simpson and E. Gregoryanz, *Nat. Mater.*, 2015, **14**, 495–499.
18 C. J. Pickard and R. J. Needs, *Nat. Phys.*, 2007, **3**, 473–476.
19 C. J. Pickard and R. J. Needs, *Phys. Status Solidi B*, 2009, **246**, 536–540.
20 C. J. Pickard, M. Martinez-Canales and R. J. Needs, *Phys. Rev. B: Condens. Matter Mater. Phys.*, 2012, **85**, 214114.
21 B. Monserrat, R. J. Needs, E. Gregoryanz and C. J. Pickard, *Phys. Rev. B*, 2016, **94**, 134101.
22 B. Monserrat, N. D. Drummond, P. Dalladay-Simpson, R. T. Howie, P. López Ríos, E. Gregoryanz, C. J. Pickard and R. J. Needs, *Phys. Rev. Lett.*, 2018, **120**, 255701.
23 J. M. McMahon and D. M. Ceperley, *Phys. Rev. Lett.*, 2011, **106**, 165302.
24 H. Y. Geng, H. X. Song, J. F. Li and Q. Wu, *J. Appl. Phys.*, 2012, **111**, 063510.
25 H. Liu, H. Wang and Y. Ma, *J. Phys. Chem. C*, 2012, **116**, 9221–9226.

26 H. Y. Geng, Q. Wu and Y. Sun, *J. Phys. Chem. Lett.*, 2017, **8**, 223–228.

27 P. Loubeyre, F. Occelli and P. Dumas, *Phys. Rev. B: Condens. Matter Mater. Phys.*, 2013, **87**, 134101.

28 C. S. Zha, R. E. Cohen, H. K. Mao and R. J. Hemley, *Proc. Natl. Acad. Sci. U. S. A.*, 2014, **111**, 4792–4797.

29 S. Azadi, R. Singh and T. D. Kühne, *J. Comput. Chem.*, 2018, **39**, 262–268.

30 C. Ji, B. Li, W. Liu, J. S. Smith, A. Majumdar, W. Luo, R. Ahuja, J. Shu, J. Wang, S. Sinogeikin, Y. Meng, V. B. Prakapenka, E. Greenberg, R. Xu, X. Huang, W. Yang, G. Shen, W. L. Mao and H.-K. Mao, *Nature*, 2019, **573**(7775), 558–562.

31 J. P. Perdew, K. Burke and M. Ernzerhof, *Phys. Rev. Lett.*, 1996, **77**, 3865–3868.

32 S. Azadi and W. M. C. Foulkes, *Phys. Rev. B: Condens. Matter Mater. Phys.*, 2013, **88**, 014115.

33 S. Azadi and G. J. Ackland, *Phys. Chem. Chem. Phys.*, 2017, **19**, 21829–21839.

34 J. McMinis, R. C. Clay, D. Lee and M. A. Morales, *Phys. Rev. Lett.*, 2015, **114**, 105305.

35 J. Klimeš, D. R. Bowler and A. Michaelides, *J. Phys.: Condens. Matter*, 2010, **22**, 022201.

36 M. Dion, H. Rydberg, E. Schröder, D. C. Langreth and B. I. Lundqvist, *Phys. Rev. Lett.*, 2004, **92**, 246401.

37 K. Lee, E. D. Murray, L. Kong, B. I. Lundqvist and D. C. Langreth, *Phys. Rev. B: Condens. Matter Mater. Phys.*, 2010, **82**, 081101(R).

38 M. A. Morales, J. M. McMahon, C. Pierleoni and D. M. Ceperley, *Phys. Rev. B: Condens. Matter Mater. Phys.*, 2013, **87**, 184107.

39 R. C. Clay, J. McMinis, J. M. McMahon, C. Pierleoni, D. M. Ceperley and M. A. Morales, *Phys. Rev. B: Condens. Matter Mater. Phys.*, 2014, **89**, 184106.

40 Y. Wang, J. Lv, L. Zhu and Y. Ma, *Phys. Rev. B: Condens. Matter Mater. Phys.*, 2010, **82**, 094116.

41 Y. Chen, H. Y. Geng, X. Yan, Y. Sun, Q. Wu and X. Chen, *Inorg. Chem.*, 2017, **56**, 3867–3874.

42 X. Zhong, L. Yang, X. Qu, Y. Wang, J. Yang and Y. Ma, *Inorg. Chem.*, 2018, **57**, 3254–3260.

43 Y. Wang, J. Lv, L. Zhu and Y. Ma, *Comput. Phys. Commun.*, 2012, **183**, 2063–2070.

44 G. Kresse and J. Furthmüller, *Phys. Rev. B: Condens. Matter Mater. Phys.*, 1996, **54**, 11169–11186.

45 P. E. Blöchl, *Phys. Rev. B: Condens. Matter Mater. Phys.*, 1994, **50**, 17953–17979.

46 G. Kresse and D. Joubert, *Phys. Rev. B: Condens. Matter Mater. Phys.*, 1999, **59**, 1758–1775.

47 H. J. Monkhorst and J. D. Pack, *Phys. Rev. B: Solid State*, 1976, **13**, 5188–5192.

48 P. Giannozzi, S. de Gironcoli, P. Pavone and S. Baroni, *Phys. Rev. B: Condens. Matter Mater. Phys.*, 1991, **43**, 7231–7242.

49 K. Parlinski, Z. Q. Li and Y. Kawazoe, *Phys. Rev. Lett.*, 1997, **78**, 4063–4066.

50 A. Togo and I. Tanaka, *Scr. Mater.*, 2015, **108**, 1–5.

51 S. J. Clark, M. D. Segall, C. J. Pickard, P. J. Hasnip, M. I. J. Probert, K. Refson and M. C. Payne, *Z. Kristallogr.*, 2005, **220**, 567–570.

52 J. S. Lin, A. Qteish, M. C. Payne and V. Heine, *Phys. Rev. B: Condens. Matter Mater. Phys.*, 1993, **47**, 4174–4180.

53 A. Fonari and S. Stauffer, https://github.com/raman-sc/VASP/, 2013.

54 D. Porezag and M. R. Pederson, *Phys. Rev. B: Condens. Matter Mater. Phys.*, 1996, **54**, 7830–7836.

55 N. D. Drummond, B. Monserrat, J. H. Lloyd-Williams, P. Lòpez Rìos, C. J. Pickard and R. J. Needs, *Nat. Commun.*, 2015, **6**, 7794.

56 P. Loubeyre, F. Occelli and P. Dumas, *Nature*, 2020, **577**, 631–635.

57 I. B. Magdău and G. J. Ackland, *Phys. Rev. B: Condens. Matter Mater. Phys.*, 2013, **87**, 174110.

58 I. B. Magdău and G. J. Ackland, *J. Phys.: Conf. Ser.*, 2014, **500**, 032012.

59 G. J. Ackland and I. B. Magdău, *High Pressure Res.*, 2014, **34**, 198–204.